Pipe-diffusion-enriched dislocations and interfaces in SnSe/PbSe heterostructures

Eamonn T. Hughes,[1] Brian B. Haidet,[1] Bastien Bonef,[1] Wei Cai,[2,3] and Kunal Mukherjee[3,*]
[1]*Materials Department, University of California, Santa Barbara, Santa Barbara, California 93106, USA*
[2]*Department of Mechanical Engineering, Stanford University, Stanford, California 94305, USA*
[3]*Department of Materials Science and Engineering, Stanford University, Stanford, California 94305, USA*

(Received 7 January 2021; accepted 8 July 2021; published 27 July 2021)

Dislocations provide fast diffusion pathways for atoms in semiconductors which can alter compositional profiles of finely tuned heterostructures. We show in model lattice-mismatched IV-VI semiconductor heterostructures of SnSe/PbSe on GaAs substrates that threading dislocations are highly enriched with group IV species of the neighboring layer, with artifacts that reflect the dynamic nature of dislocations when growing dissimilar materials as well as altered bonding properties at the dislocation core. Using atom probe tomography, we characterize one-dimensional nanometer-wide Sn-enriched filaments, which extend downward from SnSe through threading dislocations in the PbSe layer and infiltrate the remote PbSe/GaAs interface through the misfit dislocation network in the short time of growth. Local Sn compositions of only 6%–8% around the dislocations are significantly lower than the 30% Sn expected in bulk PbSe. We estimate the diffusivity of Sn atoms along threading dislocations to be 10^{-14} cm^2 s^{-1} at 300 °C, approximately three orders of magnitude larger than the lattice diffusivity. In contrast, Pb atoms from PbSe either do not diffuse upward into the orthorhombic SnSe layer or do so only a short distance as one-dimensional filaments before abruptly stopping, likely due to the nature of SnSe on PbSe epitaxy involving lattice mismatch. Beyond compositional anomalies, we detect elevated multiple-atom evaporation events that are spatially correlated to the dislocation, over and above an already high baseline in the matrix. In mixed-bonded IV-VI materials, where previous work has linked such events to the nature of bonding, we find that dislocations show up as distinct from the matrix.

DOI: 10.1103/PhysRevMaterials.5.073402

I. INTRODUCTION

Dislocations are widely known to degrade the electronic properties of semiconductors. These line defects in the crystal structure introduce long-range strain fields and isolated states within the band gap that increase both carrier scattering and recombination. Less known is that dislocations can also locally alter the composition of a device either by segregation of species around the core [1–3] or by fast diffusion along the core [4,5]. This second phenomenon, known as short-circuit or pipe diffusion, enables transport of atoms between layers of a heterostructure, which alters the intended device design. The resultant negative effects have been well documented across a broad range of semiconductor materials systems including SiGe [6,7], HgCdTe [8,9], and III-V [10–12]. The rate of pipe diffusion correlates to the rate of bulk diffusion for metals, the only materials family where this has been studied in detail [13]. Hence, we expect pipe diffusion to be particularly important for materials and devices where either (i) the bulk diffusivity is high or (ii) the dislocation density is often high. The IV-VI (Pb,Sn,Ge)-(S,Se,Te) family of chalcogenide semiconductors meets both criteria. They are soft materials with unique interatomic bonding and are used in devices with dislocation densities in the range of 10^7–10^9/cm^2 due to incompatible substrates and challenging growth. Such thin films of IV-VI materials have found use as infrared photodetectors and light emitters [14,15] and as thermoelectric materials [16,17]. More recently, certain IV-VI materials have also shown promise in phase-change devices [18] and as quantum materials hosting topologically nontrivial states [19,20]. We think the possibility of an altered composition at the dislocation core will be highly relevant to all applications of IV-VI materials where charge carrier scattering and recombination is important.

The detailed compositional environment surrounding dislocations in a semiconductor heterostructure is difficult to study by characterization techniques such as secondary ion mass spectrometry (SIMS) or energy dispersive x-ray spectroscopy (EDS) in a transmission electron microscope (TEM), as neither of these techniques simultaneously provides high spatial resolution and high compositional sensitivity. While SIMS has been instrumental in foundational studies of pipe diffusion [21–24], atom probe tomography (APT) offers dramatically improved lateral spatial resolution enabling detailed examination of the compositional environment surrounding individual dislocations [25–27]. With relevance to phase-change properties, APT was recently shown to inform on the nature of bonding in chalcogenide materials following an analysis of field-evaporation characteristics [28]. In this paper, we study pipe diffusion in a SnSe/PbSe heterostructure grown on lattice-mismatched GaAs using APT. We find that both Sn and Pb atoms rapidly diffuse through threading dislocations even in the short time spent at the relatively low growth temperature. The morphology of the compositional filaments formed by pipe diffusion additionally reflects the dynamic

*kunalm@stanford.edu

nature of dislocations in the growing lattice-mismatched film. Finally, we present preliminary evidence for modified bonding at dislocations through an analysis of APT field evaporation.

II. EXPERIMENTAL METHODS

Sample preparation. We grew SnSe/PbSe heterostructures in a Riber Compact 21 system by molecular beam epitaxy (MBE) on (001)-oriented GaAs substrates prepared via a regrowth and arsenic capping process performed in a Veeco GEN III MBE system. After removing the arsenic cap, the GaAs surface was exposed to compound PbSe flux from a PbSe effusion cell for 30 s at 400 °C to modify the surface and seed a (001)-oriented film [29]. The substrate was then cooled to 330 °C to nucleate and coalesce a thin layer of (001) PbSe. The remainder of the 80 nm PbSe layer was grown at 300 °C followed immediately by a 200 nm SnSe layer using a SnSe compound effusion cell. Additionally, a second similar heterostructure was grown but with a thinner 15 nm PbSe layer. These two heterostructures are referred to as "thick structure" and "thin structure" throughout the paper.

Sharpened conical tips from these samples were prepared for atom probe tomography (APT) using a FEI Helios 600 focused ion beam (FIB) microscope by successive 30 kV annular milling steps and a final 2 kV broad-area mill to reduce high-energy ion-beam damage and form the final tip shape. Although the specimen diameter is quite small, about 10 nm at the apex and 100 nm at the base, the threading dislocation densities in these structures are high enough ($>10^9$ cm^{-2}) such that a randomly extracted site has a reasonable probability of containing a threading dislocation.

Characterization. APT tips were evaporated at 35 K using a Cameca 3000X HR local electrode atom probe (LEAP) in voltage pulsing mode with a pulse fraction of 25% and at a relatively slow 75 kHz or lower repetition rate to allow for accurate detection of heavy ion complexes. Note that while most semiconductor materials require laser pulsing for successful evaporation, the narrow-gap IV-VI materials, much like metals, can be evaporated by voltage pulsing, which can reduce compositional artifacts and improve resolution. The target evaporation rate—the average number of ions evaporated per pulse—ranged from 0.005 to 0.01. This low rate is generally intended to minimize the probability of multiple evaporation events; however, the bonding nature of these materials leads to very high rates of multiple events regardless of the evaporation rate. Finally, dataset reconstruction was performed using IVAS software by measuring the preevaporation tip profile and using interface flatness to evaluate reconstruction fidelity. See Fig. S1 in the Supplemental Material for a mass spectrum from both structure types [30]. Finally, cross-sectional scanning transmission electron microscopy (STEM) was performed on FIB-prepared foils from each structure using a FEI Talos STEM.

III. RESULTS AND DISCUSSION

A. Sample structure

The heterostructures investigated here comprise layers with dissimilar crystal structures, which leads to an unusual dislocation morphology. The GaAs (substrate) is zinc blende (cubic); the PbSe interlayer is rocksalt (cubic), which is 8% larger in lattice constant than GaAs; and the SnSe epilayer is *Pnma* (orthorhombic) and forms a layered structure with intralayer covalent bonding and interlayer van der Waals bonding that is also lattice mismatched to PbSe. Despite these crystal structure and lattice constant mismatches, each layer grows epitaxially on the previous one as indicated by symmetric XRD scans shown in Figs. S2(a) and S2(b) in the Supplemental Material [30]. A reciprocal space map (RSM) of the (10 0 1) and (10 1 0) planes of SnSe (Figs. S3(b) [30]) indicates that this layer consists of two orientations in roughly equal proportions, with either the [010] or [001] SnSe axis aligned to PbSe [110], but in both cases the [100] SnSe axis is aligned to PbSe [001] [30]; these 45 ° oppositely rotated SnSe grains on PbSe minimize epitaxial strain due to the +2.5% and −4.4% in-plane lattice mismatch of orthorhombic SnSe on cubic PbSe.

Cross-sectional scanning transmission electron microscopy (X STEM) of the thick structure (80 nm PbSe layer) in Fig. 1(a) reveals a high threading dislocation density in the PbSe layer. This results from three-dimensional island nucleation of rocksalt PbSe on zinc-blende GaAs combined with the compressive lattice mismatch, which together generate a network of short, closely spaced misfit dislocations and accompanying threading dislocations, on the order of 10^{10} cm^{-2} [29]. Because the primary slip system in PbSe is $\{100\}\langle 110\rangle$, resolved misfit shear on these slip planes is zero, so threading dislocations are largely immobile in the PbSe layer. This inhibits dislocation fusion and annihilation reactions, barring any secondary slip or dislocation climb activity, so the high initial threading dislocation density persists through the thin PbSe interlayer. Entering the SnSe epilayer, the threading dislocation density drops noticeably as new misfit dislocations form at the interface to relieve lattice-mismatch strain. Indeed, there are several instances in Fig. 1(a) of threading dislocations in PbSe or SnSe that appear to terminate or originate, respectively, at the SnSe/PbSe interface as they bend laterally to form misfit dislocation segments. The network of misfit and threading dislocations is summarized by the sketch in Fig. 1(b). Due to the high density of dislocations, this epitaxial heterostructure represents a model system for studying accelerated diffusion by APT.

B. Dislocation-enhanced diffusion of tin

We first examine the diffusion behavior of Sn through threading dislocations in PbSe. Figures 2(a) and 2(b) show two perpendicular {110} projections of an APT tip from the thick PbSe layer structure revealing two distinct Sn-enriched filaments, with one slightly curved and cut off at the edge of the tip. The line direction of the straight filament is comparable to that of threading dislocations seen by STEM in Fig. 1(a), implying that these filaments form by downward pipe diffusion of Sn atoms through a threading dislocation. Note that these maximum composition projections or tracer method [2] projections—a technique which projects the maximum composition of a single species along a certain direction through the sample thickness onto the image plane—are composited to display the minority group-IV species in each

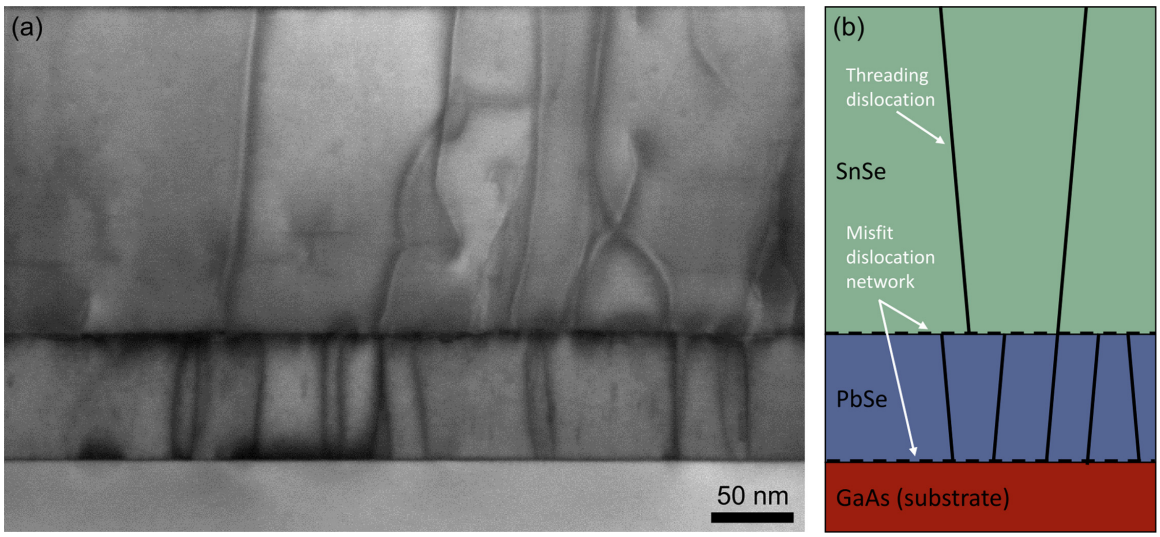

FIG. 1. (a) Bright-field scanning transmission electron microscopy (BF STEM) image of the thick PbSe layer structure showing the high density of threading dislocations present in both the PbSe and SnSe layers and misfit dislocations located at the interfaces. The two-beam condition is $g = 004$. (b) Sketch of the structure showing misfit dislocations at interfaces and their associated threading dislocations.

layer; i.e., Pb composition is shown in the SnSe layer and Sn is shown in PbSe and below, which helps to illustrate the interdiffusion behavior. These dislocations appear to supply Sn atoms to the PbSe/GaAs interface, where they spread out across the interface aided by the high-density network of misfit dislocations located there. Based on the expected misfit dislocation spacing of 4–5 nm in both directions and the limited lateral resolution of APT particularly at this interface, it seems plausible that the interfacial Sn composition would appear smoothly distributed rather than concentrated along misfit dislocation lines. Figures 2(c) and 2(d) show similar instances of this Sn-diffusion behavior from the structure where the PbSe layer is only 15 nm (thin structure).

Examining the diffusion behavior of Sn in more detail, Fig. 2(e) plots the composition profile along the straight dislocation in the thick structure [Figs. 2(a) and 2(b)] and compares it to a control region away from the dislocation. One particularly surprising feature of the dislocation composition profile is the sharp drop-off in Sn composition across the SnSe/PbSe interface, rapidly declining from nearly 90% (group IV site) on the SnSe side to less than 10% on the PbSe side over just a few nanometers. After this, the profile only gently slopes downward, indicating this original large drop-off is not the result of a diffusion limit, but rather an incorporation limit.

Rocksalt PbSe can substitutionally accommodate roughly 30% Sn at 300 °C [31–33], so the smaller observed ∼8% Sn incorporation limit is surprising. Given the smaller size of the Sn atoms, the PbSnSe filament should be strained tensile; however, as detailed in a calculation of the equilibrium solubility around a dislocation core with mismatch strain in Figs. S6 and S7 in the Supplemental Material [30] (also see [33,34]), this strain does not appear to strongly affect the equilibrium Sn composition. We find that it reduces the solubility only slightly from 29.8% under unstrained conditions to 26.5% under tensile strain. In addition to strain, there may be other energetic factors such as interfacial energies or nontrivial mechanical or electrostatic interactions with the dislocation core that result in the composition limit we observe.

Given this apparent incorporation limit, we estimate the enhanced one-dimensional (1D) diffusivity of Sn along the threading dislocation by assuming a constant composition at the SnSe/PbSe interface and fitting to the appropriate solution to the diffusion equation, $C(z) = C_0\mathrm{erfc}(\frac{z}{Dt})$, where the initial composition, C_0, is set by the Sn incorporation limit (6%–8%); t is time at growth temperature for the SnSe layer (3600 s); and z is distance below the SnSe/PbSe interface. This solution assumes diffusion into a semi-infinite body, which, given the significant Sn composition at the PbSe-GaAs interface, is not fully met, even accounting for the continued diffusion of Sn into this interface. Given these limitations, we report only a maximum possible value for enhanced diffusivity of Sn through the dislocation, which we measure to be 10^{-14} cm^2 s^{-1}. This is about three orders of magnitude larger than the lattice diffusivity of Sn atoms in similarly n-type PbSe extrapolated down to our 300 °C growth temperature [35]. This large gap between lattice diffusivity and enhanced dislocation diffusivity supports using the 1D diffusion equation since Sn primarily travels downward through the dislocation with minimal outward diffusion or loss into the surrounding material. We also verify that the lattice diffusivity of Sn atoms at dilute concentrations in PbSe away from the dislocations roughly matches the expected 300 °C lattice diffusivity of 10^{-17} cm^2 s^{-1} [35].

Looking toward the PbSe/GaAs interface, there is an apparent increase in Sn composition where the dislocation meets the interface, highlighted in Fig. 2(f). While this could indicate a higher incorporation limit for Sn near the mismatched interface, it is more likely an artifact of the composition sampling method. Each 1 nm composition slice is averaged over a 5 nm radius around the dislocation, and since the Sn composition decays radially around the dislocation, the measured average composition will slightly underestimate the maximum core composition. At the interface, however, Sn atoms spread out laterally, so we should expect a higher apparent concentration

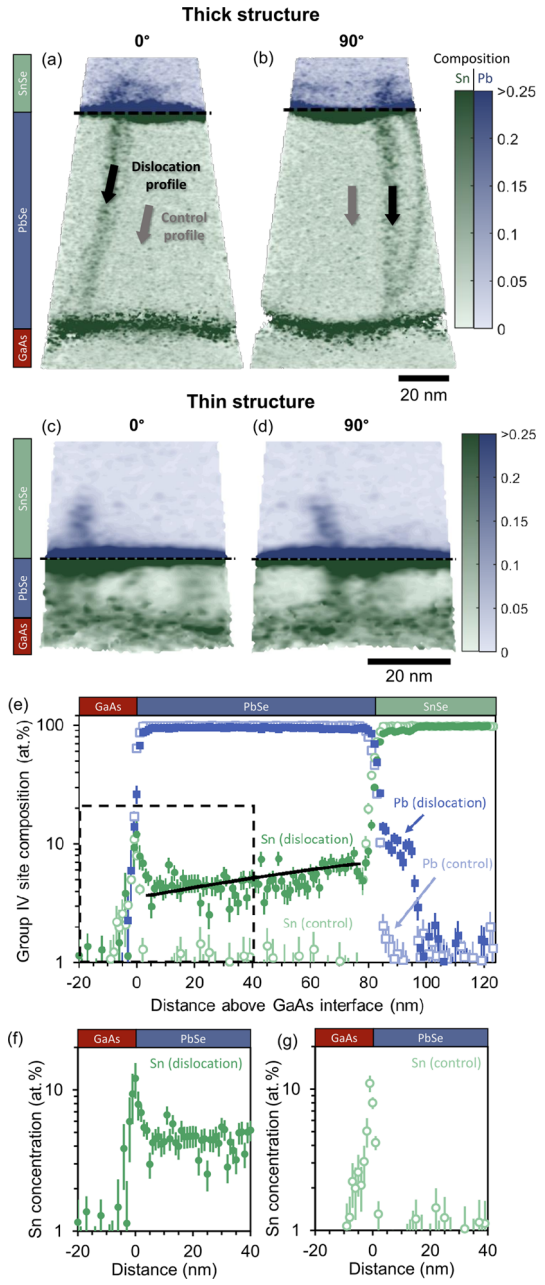

FIG. 2. (a,b) Orthogonal maximum composition projections of the APT dataset showing Sn composition in PbSe and Pb composition in SnSe. Two Sn-enriched filaments result from diffusion through threading dislocations during growth with additional accumulation of Sn at the GaAs/PbSe interface. Pb also protrudes a short distance into SnSe. (c,d) Maximum projections for a second APT dataset from the structure with a thinner PbSe layer (thin structure). There are several filaments enriched with Sn but only one short Pb-enriched filament extending into SnSe. (e) One-dimensional Sn and Pb composition profiles from the tip in (a,b). Compositions are sampled from a 5 nm radius around the threading dislocation (closed shapes) [black arrow in (a,b)] and in a control region away from the dislocation (open shapes) [gray arrows in (a,b)]. The solid line is a diffusion profile fit. (f,g) Magnified view of the boxed region in (e) showing Sn composition along the (f) dislocation and (g) control profile. The composition rise at the interface in (f) may be an artifact of the composition sampling method. In (g), the rise at the interface results from the Sn-enriched interface.

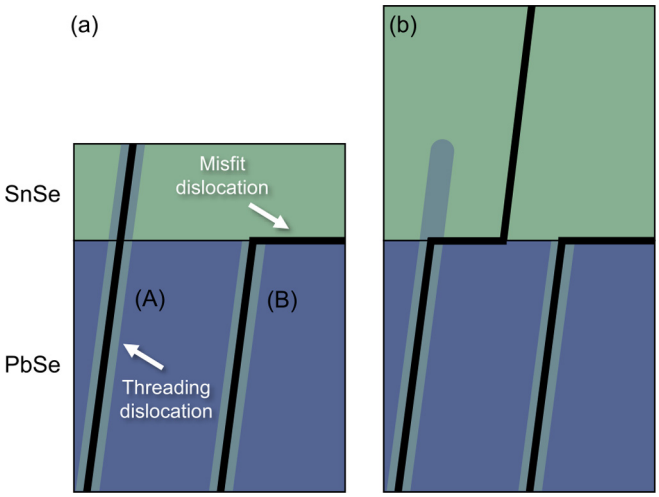

FIG. 3. Illustration of how the short Pb-enriched filament forms. (a) At the start of SnSe growth, dislocation (A) continues into SnSe enabling upward diffusion of Pb. Dislocation (B), with a different Burgers vector, bends over at the interface where it potentially fuses with another dislocation as its self-energy inside SnSe is very high. (b) After SnSe is sufficiently thick, stress fields cause dislocation (A) to glide away cutting off the initial fast diffusion pathway and leaving behind a Pb filament.

based on this alone. In the control profile [Fig. 3(g)], the rise in Sn composition at the interface is simply a reflection of the Sn-enriched interface.

The mechanism that enables diffusion of Sn atoms through PbSe has been suggested [35] to be the dissociated mechanism devised by Frank and Turnbull [36]. This allows for simultaneous rapid diffusion via interstitials and high-concentration incorporation in substitutional sites. As the material grown here is *n*-PbSe due to a slight excess of group IV, Sn should readily diffuse interstitially, but incorporation will be limited by the low equilibrium supply of group-IV site vacancies. To circumvent this limitation, the dislocation can act as a vacancy source, transporting vacancies from the crystal surface into the bulk via negative climb and incorporating Sn along the extra half plane of the dislocation.

We expect the large incorporation of Sn at dislocations to impact electrical properties. Even without compositional change, dislocations affect minority carrier devices such as photodetectors and light emitters by introducing both deep and shallow states in the gap that lead to increased generation and recombination currents in the *p*-*n* junction. The impact of this is seen in greater leakage currents in reverse bias and reduced quantum efficiency in forward bias [37]. Some groups suggest dislocations might even have metallic character that leads to a shunt resistance across the junction [38–40]. In the bulk, alloying PbSe with Sn decreases the band gap until it closes entirely at about 22% Sn (group-IV site). From Fig. 2(e), the Sn composition along the threading dislocation is about 8%, which would indicate a reduced unstrained bulk 300 K band gap of about 0.2 eV compared to 0.28 eV in PbSe, although this may underestimate the maximum possible effect since the dislocation core composition is slightly higher. While we can speculate whether some of the dislocation-related states may now end up outside the narrow gap, as

Park *et al.* say is the case in InAs, generation-recombination processes across the gap should increase regardless [41]. Going forward, it will be interesting to explore means to turn dislocation diffusion into an advantage in PbSe/PbSnSe/PbSe double heterostructures for long-wavelength light emitters. By analogy, we would expect the composition at a threading dislocation core in the PbSnSe layer to now become less Sn rich (and hence wider gap) than the surrounding matrix, which perhaps would reduce the capture of minority carriers by dislocations.

C. Diffusion behavior of lead

The heterostructure approach to the study of pipe diffusion also lets us investigate the rather unique case of upward diffusion in the growth direction. Here, diffusion occurs in a much more dynamic environment since the dislocations are being extended at the growth surface and may move. Figures 2(a)–2(d) reveal a curious short protrusion of Pb atoms into SnSe in each tip that is spatially aligned to a Sn filament below. These extend only about 10 nm above the interface, and as shown in Fig. 2(e), the composition of Pb is reasonably steady before abruptly decaying. This is unlike the longer steadier profile of Sn in PbSe and is very uncharacteristic of continuous 1D diffusion. The thin PbSe structure similarly shows an abrupt decay in Pb composition (Fig. S3 in the Supplemental Material [30]). Given the dissimilar slopes of these two short profiles, we have not attempted to extract a diffusivity.

We suggest a formation mechanism to explain these unusual Pb protrusions, depicted in Fig. 3. While growing the first layers of SnSe [Fig. 3(a)], threading dislocations with certain Burgers vectors represented by dislocation (A) from PbSe continue straight into SnSe. Pb diffuses readily upward along the dislocation, likely aided by proximity to the surface. Although there is no resolved shear on these dislocations' primary slip system from misfit stress, above a certain thickness the stress fields from other threading dislocations or from the free surface can induce glide [Fig. 3(b)], causing the threading dislocation to move and leave behind an abruptly terminating Pb-enriched filament. This mechanism is supported by the signs of misfit dislocation formation in Fig. 1(a) and the laterally aligned Pb- and Sn-enriched filaments in Figs. 2(a)–2(d). While we expect that Pb continues to diffuse upward through the threading dislocation after gliding, we have not observed this in any evaporated tip (i.e., a long Pb-rich filament without a corresponding Sn-rich filament below). This could simply reflect the lower threading dislocation density in the SnSe layer.

This mechanism explains the observed Pb filaments, but there are also many Sn filaments in PbSe that do not extend into PbSe as is clear from Figs. 4(a) and 4(b), and Figs. 4(c) and 4(d), which show lateral composition maps of Sn in PbSe and Pb in SnSe for the thick and thin PbSe structures, respectively. There are multiple distinct Sn-enriched regions both in Figs. 4(a) and 4(b) but only a single clear Pb-enriched region in Figs. 4(c) and 4(d). This can be explained by threading dislocations with different Burgers vectors to dislocation (A) [represented now by dislocation (B) in Fig. 3] immediately bending over at the interface due to unfavorable energetics in the layered orthorhombic SnSe crystal structure [42]. Given

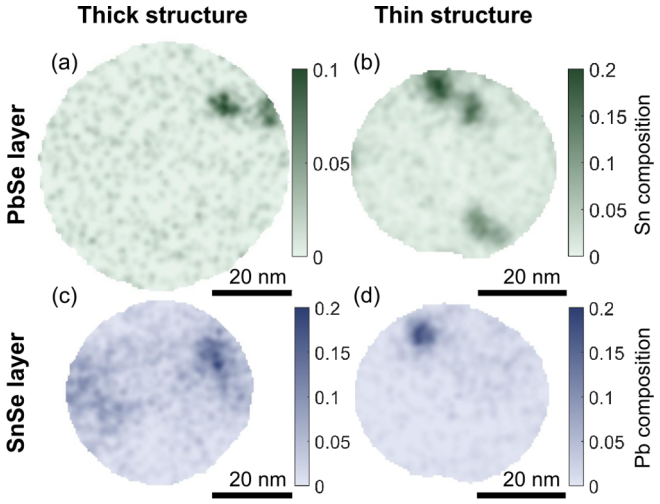

FIG. 4. (a,b) Top-view composition maps of Sn in PbSe in the structures with a (a) thick and (b) thin PbSe layer. Note that not all filaments of Sn in PbSe have a corresponding Pb filament in SnSe. (c,d) Composition maps of Pb in SnSe in the (c) thick and (d) thin structures. The Sn maps are sampled midway through the PbSe layer, and the Pb maps are sampled just above the PbSe-SnSe interface. All compositions are averaged over 5 nm in height.

the high threading dislocation density in PbSe, many dislocations fuse or annihilate during this transition, yielding a reduction in threading dislocation density in SnSe observed in Fig. 1(a). One final feature, seen in Fig. 4(b), is the broad Pb-enriched region toward the left side of the composition map, also visible in cross section in Fig. 2(b). This Pb enrichment may be a remnant of lateral Pb diffusion through a misfit dislocation lying just above the PbSe/SnSe interface. We observe an example of such a dislocation configuration by X STEM, shown in Fig. S4 in the Supplemental Material [30].

D. Probing bond character near dislocations

So far, we have shown that dislocations act as short-circuit diffusion pathways due to the altered structure surrounding their cores, but previous work suggests that APT may offer a route to probe differences in bonding at dislocations in PbSe. Wuttig *et al.*, in a series of papers, suggest that details in the APT detector event maps enable studying the nature of bonding in chalcogenide materials [18,43,44], specifically by examining the number of evaporation events where multiple ions are detected. Our observed probability of multiple evaporation events for PbSe by voltage-pulsed APT (64%) matches well with that observed for their laser-pulsed APT (62%) [44]. This unusually high probability of multiple events has been attributed to the so-called "metavalent" bonding of these structures, a sort of intermediate (but reportedly not a hybrid) bonding state between covalent, ionic, and metallic bonding where electrons are neither fully localized nor delocalized [45]. Other metavalently bonded materials show similarly high rates of multiple events such as PbTe (64%) [44,46] and PbS (64%) [44]. For SnSe and GaAs, we measure probabilities of multiple events of 90% and 30%, respectively; the latter is within expectations but the former is not and will be discussed shortly.

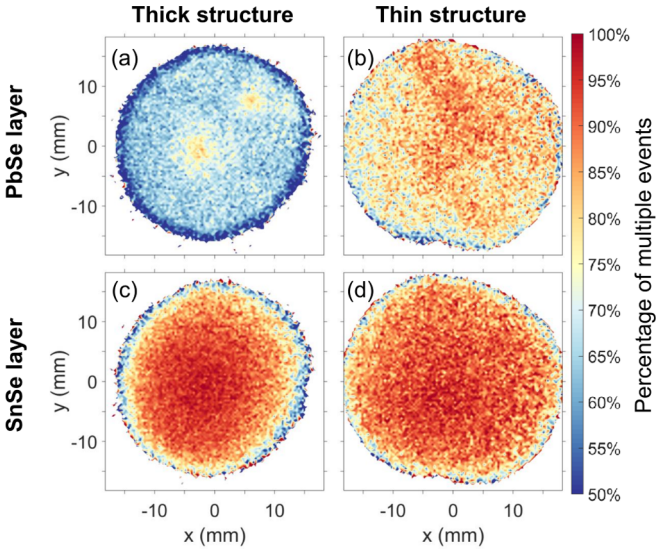

FIG. 5. Detector maps showing percentage of multiple events, i.e., the percentage of measured evaporation events where more than one ion is detected. (a,b) Multiple events from the PbSe layer of the APT tips from the (a) thick (500 000 ions) and (b) thin structure (250 000 ions). The elevated multiple hit regions in (a) and (b) are due to the threading dislocations present there. The central elevated regions are unrelated to threading dislocations. (c,d) Multiple events from the SnSe layer of the APT tips from the (c) thick and (d) thin structures (250 000 ions each). These are collected from the bottom of the SnSe layer to capture the Pb-enriched filaments, but they do not appear to affect the probability of multiple events.

In Fig. 5, we examine the spatial distribution of multiple evaporation events across the two-dimensional APT detector for different layers of the two structures examined (thick and thin structure). Figure 5(a), the map from the PbSe layer of the thick structure, has two spikes in multiple-events percentage: one near the center corresponding to the 001 pole that is commonly seen [47,48], but also a second one in the upper-right quadrant of the detector. Looking back at Fig. 4(a), this matches with the location of the two Sn-enriched threading dislocations in that structure. The multiple-event map for the thin structure [Fig. 5(b)] also shows increased multiple events corresponding to the Sn-enriched regions from Fig. 4(c). In this case, the correlation is somewhat obscured by an elevated background level of multiple events, which we attribute to proximity to interfaces containing misfit dislocations in this thin structure. To verify that these correlations are not simply coincidental, Fig. S5(a) shows a comparable multiple-event map for a tip without Sn filaments, and as expected, there is only a single central elevated multiple-event region at the [001] pole like that of Fig. 5(a) [30].

One possible explanation for the increased multiple events around dislocations in PbSe is the Sn enrichment that accompanies them. Since SnSe evaporates with a higher percentage of multiple events than PbSe, alloying PbSe with Sn might be expected to raise its multiple-event percentage. However, the exceptionally high multiple evaporation rate of SnSe is likely attributable to its layered structure and orientation, which is irrelevant when alloyed in small amounts in PbSe as the structure remains cubic rocksalt. Additionally, if this effect were dominant, there would likely also be a corresponding drop in multiple events around the short Pb filaments at the bottom of the SnSe layers. However, Figs. 5(c) and 5(d), sampled from the very bottom of the SnSe layer, show no indication of decreased multiple events in the Pb-enriched regions corresponding to Figs. 4(b) and 4(d). They look qualitatively similar to a tip with no Pb filament (Fig. S5(b) in the Supplemental Material [30]). A more plausible explanation is that, rather than a compositional effect, the enhanced multiple events around threading dislocations are a result of the altered bonding of the dislocation itself. This accounts for the lack of altered multiple events in the SnSe layers [Figs. 5(c) and 5(d)] since the threading dislocations have glided away from here by the mechanism discussed in Fig. 3.

Stepping back from dislocations to consider bulk properties, covalently bonded semiconductors such as Si and GaAs tend to evaporate with very few multiple events. Recently, this has been said to translate to layered materials with intralayer covalent bonds despite their interlayer van der Waals bonding. GeSe, which has the same layered structure as SnSe [28], has been observed to evaporate with only a 13.3% probability of multiple events by laser-pulsed APT of sputter-deposited films [18]. Our observation of an extremely high 90% probability of multiple events in SnSe is at odds with this result. We think that the orientation of layered films with respect to the electric field in the APT tip may play a discriminating role here. The covalently bonded layers of sputter-deposited GeSe could have been more closely aligned parallel to the axis of the tip, whereas the epitaxial SnSe layers in our study here are known to be aligned perpendicular to the tip axis and thus may be easier to delaminate and generate enhanced multiple events. APT already provides rich crystallographic information [47] in addition to a compositional picture, but now the prospect of obtaining localized bonding information is indeed intriguing and should be investigated further.

IV. SUMMARY AND CONCLUSIONS

The prospect of novel functionality is driving the development of heterostructures composed of increasingly dissimilar materials. At the same time, our understanding of the defects that arise in such heterostructures needs to keep pace. The versatile IV-VI material system allows for the creation of unique heterostructures with broad application in a number of technical fields. We have shown in such a system that Sn atoms readily diffuse into PbSe via pipe diffusion through threading dislocations and can even enrich remote interfaces through misfit dislocation networks. Yet, we have more work to do to uncover factors beyond simple misfit strain that set solubility limits at dislocation cores for otherwise greatly miscible atoms. Pb atoms also readily diffuse into orthorhombic SnSe but only a short distance, which we propose is an artifact of threading dislocations gliding away and cutting off the fast diffusion pathway. Additionally, not all Sn-enriched dislocation filaments have a corresponding filament of Pb directly above them, possibly due to differences in how dislocations with different Burgers vectors transition from the rocksalt PbSe structure to the *Pnma* (orthorhombic) SnSe structure. Finally, while evaporating these structures by APT, we observe an increased probability of multiple events around the

Sn filaments but not the Pb filaments, suggesting that this effect is due to the altered bonding surrounding the dislocation rather than altered composition. The overall probability of multiple events for PbSe closely matches previously measured values, but for SnSe the measured value is far higher than what has been seen in similar structures. These results highlight the compositional changes in IV-VI heterostructures resulting from pipe diffusion, which can be easily overlooked given that many IV-VI devices operate successfully with high dislocation densities. Structure-property relations of dislocations are not yet known in semiconductors at the level where we can control and tune their properties. Better understanding these compositional changes is therefore essential for improving heterostructure design and potentially harnessing the resultant properties of these one-dimensional defects.

ACKNOWLEDGMENTS

We thank T.E. Mates and J.S. Speck for support in APT experiments and L.J. Lauhon for helpful discussions. We also would like to acknowledge K. Olsson and J. English for their MBE expertise and support. The research reported here was supported by the National Science Foundation (NSF) Materials Research Science and Engineering Center (MRSEC) at UC Santa Barbara through Grant No. DMR 1720256 (Seed). We acknowledge the use of shared facilities of the National Science Foundation (NSF) Materials Research Science and Engineering Center (MRSEC) at UC Santa Barbara, Grant No. DMR 1720256. K.M. acknowledges support from the National Science Foundation CAREER award under Grant No. DMR-1945321

[1] M. Kuzmina, M. Herbig, D. Ponge, S. Sandlöbes, and D. Raabe, Linear complexions: Confined chemical and structural states at dislocations, Science **349**, 1080 (2015).

[2] M. K. Miller, Atom probe tomography characterization of solute segregation to dislocations, Microsc. Res. Tech **69**, 359 (2006).

[3] X. Zhou, J. R. Mianroodi, A. K. Da Silva, T. Koenig, G. B. Thompson, P. Shanthraj, D. Ponge, B. Gault, B. Svendsen, and D. Raabe, The hidden structure dependence of the chemical life of dislocations, Sci. Adv. **7**, eabf0563 (2021).

[4] F. Barson, M. S. Hess, and M. M. Roy, Diffusion pipes in silicon *npn* structures, J. Electrochem. Soc. **116**, 304 (1969).

[5] T. E. Volin, K. H. Lie, and R. W. Balluffi, Measurement of rapid mass transport along individual dislocations in aluminum, Acta Metall. **19**, 263 (1971).

[6] J. G. Fiorenza, G. Braithwaite, C. W. Leitz, M. T. Currie, J. Yap, F. Singaporewala, V. K. Yang, T. A. Langdo, J. Carlin, M. Somerville, A. Lochtefeld, H. Badawi, and M. T. Bulsara, Film thickness constraints for manufacturable strained silicon CMOS, Semicond. Sci. Technol. **19**, L4 (2004).

[7] H. C.-H. Wang, Y.-P. Wang, S.-J. Chen, C.-H. Ge, S. M. Ting, J.-Y. Kung, R.-L. Hwang, H.-K. Chiu, L. C. Sheu, P.-Y. Tsai, L.-G. Yao, S.-C. Chen, H.-J. Tao, Y.-C. Yeo, W.-C. Lee, and C. Hu, Substrate-strained silicon technology: Process integration [CMOS technology], in *IEEE International Electron Devices Meeting 2003* (IEEE, Piscataway, NJ, 2003).

[8] I. M. Baker and C. D. Maxey, Summary of HgCdTe 2D array technology in the U.K, J. Electron. Mater. **30**, 682 (2001).

[9] M. A. Kinch, R. L. Strong, and C. A. Schaake, $1/f$ noise in HgCdTe focal-plane arrays, J. Electron. Mater. **42**, 3243 (2013).

[10] G. R. Woolhouse, Degradation in injection lasers, IEEE J. Quantum Electron. **11**, 556 (1975).

[11] Y. Kim, M. S. Kim, S. K. Min, and C. Lee, Dislocation-accelerated diffusion of Si in delta-doped GaAs grown on silicon substrates by metalorganic chemical vapor deposition, J. Appl. Phys. **69**, 1355 (1991).

[12] T. Egawa, T. Jimbo, Y. Hasegawa, and M. Umeno, Optical and electrical degradations of GaAs-based laser diodes grown on Si substrates, Appl. Phys. Lett. **64**, 1401 (1994).

[13] R. W. Balluffi, S. M. Allen, and W. C. Carter, *Kinetics of Materials* (Wiley, Hoboken, NJ, 2005).

[14] A. Muñoz, J. Meléndez, M. C. Torquemada, M. T. Rodrigo, J. Cebrián, A. J. De Castro, J. Meneses, M. Ugarte, F. López, G. Vergara, J. L. Hernández, J. M. Martín, L. Adell, and M. T. Montojo, PbSe photodetector arrays for IR sensors, Thin Solid Films **317**, 425 (1998).

[15] G. Springholz, T. Schwarzl, W. Heiss, G. Bauer, M. Aigle, H. Pascher, and I. Vavra, Midinfrared surface-emitting PbSe/PbEuTe quantum-dot lasers, Appl. Phys. Lett **79**, 1225 (2001).

[16] L. D. Zhao, S. H. Lo, Y. Zhang, H. Sun, G. Tan, C. Uher, C. Wolverton, V. P. Dravid, and M. G. Kanatzidis, Ultralow thermal conductivity and high thermoelectric figure of merit in SnSe crystals, Nature **508**, 373 (2014).

[17] Y. Yu, S. Zhang, A. M. Mio, B. Gault, A. Sheskin, C. Scheu, D. Raabe, F. Zu, M. Wuttig, Y. Amouyal, and O. Cojocaru-Mirédin, Ag-segregation to dislocations in PbTe-based thermoelectric materials, ACS Appl. Mater. Interfaces **10**, 3609 (2018).

[18] M. Zhu, O. Cojocaru-Mirédin, A. M. Mio, J. Keutgen, M. Küpers, Y. Yu, J. Y. Cho, R. Dronskowski, and M. Wuttig, Unique bond breaking in crystalline phase change materials and the quest for metavalent bonding, Adv. Mater. **30**, 1706735 (2018).

[19] Y. Tanaka, Z. Ren, T. Sato, K. Nakayama, S. Souma, T. Takahashi, K. Segawa, and Y. Ando, Experimental realization of a topological crystalline insulator in SnTe, Nat. Phys. **8**, 800 (2012).

[20] P. Dziawa, B. J. Kowalski, K. Dybko, R. Buczko, A. Szczerbakow, M. Szot, E. Łusakowska, T. Balasubramanian, B. M. Wojek, M. H. Berntsen, O. Tjernberg, and T. Story, Topological crystalline insulator states in $Pb_{1-x}Sn_xSe$, Nat. Mater. **11**, 1023 (2012).

[21] Y. Tajima, K. Kijima, and W. D. Kingery, Diffusion of ion implanted aluminum in silicon carbide, J. Chem. Phys. **77**, 2592 (1982).

[22] B. Y. Tong, X. W. Wu, G. R. Yang, and S. K. Wong, Study of hydrogen diffusion in crystalline silicon by secondary-ion mass spectrometry, Can. J. Phys. **67**, 379 (1989).

[23] S. J. Pearton, H. Cho, J. R. LaRoche, F. Ren, R. G. Wilson, and J. W. Lee, Oxygen diffusion into SiO_2-capped GaN during annealing, Appl. Phys. Lett. **75**, 2939 (1999).

[24] T. Nakagawa, A. Nakamura, I. Sakaguchi, N. Shibata, K. P. D. Lagerlöf, T. Yamamoto, H. Haneda, and Y. Ikuhara, Oxygen pipe diffusion in sapphire basal dislocation, J. Ceram. Soc. Jpn. **114**, 1013 (2006).

[25] B. Bonef, R. D. Shah, and K. Mukherjee, Fast diffusion and segregation along threading dislocations in semiconductor heterostructures, Nano Lett. **19**, 1428 (2019).

[26] J. Nicolas, S. Assali, S. Mukherjee, A. Lotnyk, and O. Moutanabbir, Dislocation pipe diffusion and solute segregation during the growth of metastable GeSn, Cryst. Growth Des. **20**, 3493 (2020).

[27] W. Yi, A. Kumar, J. Uzuhashi, T. Kimura, R. Tanaka, S. Takashima, M. Edo, Y. Yao, Y. Ishikawa, J. Chen, T. Ohkubo, T. Sekiguchi, and K. Hono, Mg diffusion and activation along threading dislocations in GaN, Appl. Phys. Lett **116**, 242103 (2020).

[28] M. Raghuwanshi, O. Cojocaru-Mirédin, and M. Wuttig, Investigating bond rupture in resonantly bonded solids by field evaporation of carbon nanotubes, Nano Lett. **20**, 116 (2020).

[29] B. B. Haidet, E. T. Hughes, and K. Mukherjee, Nucleation control and interface structure of rocksalt PbSe on (001) zincblende III-V surfaces, Phys. Rev. Mater. **4**, 033402 (2020).

[30] See Supplemental Material at http://link.aps.org/supplemental/10.1103/PhysRevMaterials.5.073402 for information on APT mass spectra, reciprocal space maps of the thin films, additional composition profiles and TEM images, and a calculation of the Sn solubility limit at the dislocation core.

[31] H. Krebs, K. Grün, and D. Kallen, Mischkristallsysteme zwischen halbleitenden chalkogeniden der vierten hauptgruppe, Z. Anorg. Allg. Chem. **312**, 307 (1961).

[32] J. C. Woolley and O. Berolo, Phase studies of the $Pb_{1-x}Sn_xSe$ alloys, Mater. Res. Bull. **3**, 445 (1968).

[33] A. A. Volykhov, V. I. Shtanov, and L. V. Yashina, Phase relations between germanium, tin, and lead chalcogenides in pseudobinary systems containing orthorhombic phases, Inorg. Mater. **44**, 345 (2008).

[34] T. Mura, Isotropic Inclusions, in *Micromechanics of Defects in Solids*, edited by T. Mura (Springer Netherlands, Dordrecht, 1987), pp. 74–128.

[35] G. Pineau, H. Scherrer, and S. Scherrer, Heterodiffusion of tin in *N*-type PbSe, Phys. Lett. A **75**, 234 (1980).

[36] C. Frank and D. Turnbull, Mechanism of diffusion of copper in germanium, Phys. Rev. **104**, 617 (1956).

[37] L. M. Giovane, H. C. Luan, A. M. Agarwal, and L. C. Kimerling, Correlation between leakage current density and threading dislocation density in SiGe *p-i-n* diodes grown on relaxed graded buffer layers, Appl. Phys. Lett. **78**, 541 (2001).

[38] H. Zogg, K. Alchalabi, D. Zimin, K. Kellermann, and W. Buttler, Two-dimensional monolithic lead chalcogenide infrared sensor array on silicon read-out chip, Nucl. Instrum. Methods Phys Res., Sect. A **512**, 440 (2003).

[39] A. Fach, J. John, P. Müller, C. Paglino, and H. Zogg, Material properties of $Pb_{1-x}Sn_xSe$ epilayers on Si and their correlation with the performance of infrared photodiodes, J. Electron. Mater. **26**, 873 (1997).

[40] M. Kittler, M. Reiche, B. Schwartz, H. Uebensee, H. Kosina, Z. Stanojevic, O. Baumgartner, and T. Ortlepp, Transport of charge carriers along dislocations in Si and Ge, Phys Status Solidi A **216**, 1900287 (2019).

[41] J. S. Park, J. Kang, J. H. Yang, W. E. McMahon, and S. H. Wei, Polymerization of defect states at dislocation cores in InAs, J. Appl. Phys. **119**, 045706 (2016).

[42] B. W. Dodson, Dislocation filtering: Why it works, when it doesn't, J. Electron. Mater. **19**, 503 (1990).

[43] Y. Cheng, O. Cojocaru-Mirédin, J. Keutgen, Y. Yu, M. Küpers, M. Schumacher, P. Golub, J. Y. Raty, R. Dronskowski, and M. Wuttig, Understanding the structure and properties of sesquichalcogenides (i.e., V_2VI_3 or Pn_2Ch_3 (Pn = pnictogen, Ch = chalcogen) compounds) from a bonding perspective, Adv. Mater. **31**, 1904316 (2019).

[44] S. Maier, S. Steinberg, Y. Cheng, C. F. Schön, M. Schumacher, R. Mazzarello, P. Golub, R. Nelson, O. Cojocaru-Mirédin, J. Y. Raty, and M. Wuttig, Discovering electron-transfer-driven changes in chemical bonding in lead chalcogenides (Pb*X*, where X = Te, Se, S, O), Adv. Mater. **32**, 2005533 (2020).

[45] M. Wuttig, V. L. Deringer, X. Gonze, C. Bichara, and J.-Y. Raty, Incipient metals: Functional materials with a unique bonding mechanism, Adv. Mater. **30**, 1803777 (2018).

[46] I. D. Blum, D. Isheim, D. N. Seidman, J. He, J. Androulakis, K. Biswas, V. P. Dravid, and M. G. Kanatzidis, Dopant distributions in PbTe-based thermoelectric materials, J. Electron. Mater. **41**, 1583 (2012).

[47] L. Yao, B. Gault, J. M. Cairney, and S. P. Ringer, On the multiplicity of field evaporation events in atom probe: A new dimension to the analysis of mass spectra, Philos. Mag. Lett. **90**, 121 (2010).

[48] F. De Geuser, B. Gault, A. Bostel, and F. Vurpillot, Correlated field evaporation as seen by atom probe tomography, Surf. Sci. **601**, 536 (2007).